Progress In Electromagnetics Research B, Vol. 55, 257–276, 2013

TECHNIQUE FOR INHOMOGENEOUS PROFILES IN THE CROSS-SECTION OF THE HELICAL RECTANGULAR WAVEGUIDE

Zion Menachem* **and Saad Tapuchi**

Department of Electrical Engineering, Sami Shamoon College of Engineering, Israel

Abstract—This paper presents the technique to solve inhomogeneous profiles in the cross section of the helical rectangular waveguide. We present the technique to solve inhomogeneous dielectric profiles and the relation to the method of the propagation of electromagnetic fields along a helical waveguide with a rectangular cross section. The inhomogeneous examples will introduce for a dielectric slab, for a rectangular dielectric profile, and for a circular dielectric profile, in a rectangular metallic waveguide, in the cross section of the helical waveguide. This model is useful to improve the output results of the output power transmission in the cases of space helical waveguides, by increasing the step's angle or the radius of the cylinder. The application is useful for space helical waveguides in the microwave and the millimeter-wave regimes.

1. INTRODUCTION

The methods of curved waveguides have been proposed in the literature. The propagation in curved rectangular waveguide of general-order modes were proposed by using asymptotic expansion method [1]. An approximate method for propagation in a curved dielectric waveguide with rectangular cross section was described [2]. The method is based on Airy function and Hankel function of the second kind.

Other methods for the propagation were developed in the case of empty curved waveguide. The numerical and analytical methods were proposed for curved waveguide with a rectangular cross section [3]. Equivalent circuit for circular E-plane bends in rectangular waveguide

Received 17 September 2013, Accepted 13 October 2013, Scheduled 15 October 2013

* Corresponding author: Zion Menachem (zionm@post.tau.ac.il).

was proposed by Carle [4]. The E-plane bend is suitable for satellite beamforming network applications because it shows minimum input reflection and minimum size. The method of moments solution together with a mode-matching technique for curved waveguide was proposed for a rectangular waveguide [5]. The method is applied to study the transmission characteristics of single and cascaded curved E-plane bend and H-plane bend in a rectangular waveguide. The effect of the orientation of cascaded bends on the transmission properties can be significant, and examples to demonstrate this effect are included. A differential method for wave propagation in curved waveguides with a rectangular cross section was presented by Cornet [6].

The method of the conformal transformation for the waveguide bends was proposed by Heiblum and Harris [7]. Equivalent structures are obtained that permit solution by traditional methods of optical waveguide analysis. This method is based on the first-order approximations, expressions for the attenuation along a bend, the displacement of the wave from its position in straight waveguide, the change in the propagation constant due to the bending of the waveguide, and the transmission loss in a practical bend. Bending losses of dielectric slab optical waveguide with double or multiple claddings were proposed by Kawakami et al. [8]. The general method for calculating the change of the propagation constant of a surface-wave mode on a curved open waveguide of arbitrary cross section was proposed [9]. The resulting formulas require knowledge only of the fields and propagation constant of the corresponding straight waveguide mode, and the value of the radius of curvature of the waveguide axis. Hollow metallic and dielectric waveguides for long distance optical transmission and lasers were investigated by Marcatily and Schmeltzer [10]. Propagation in curved rectangular waveguides based on the perturbation techniques was published in the book of the electromagnetic waves and curved structures [11].

Fast-wave analysis of an inhomogeneously-loaded helix enclosed in a cylindrical waveguide has been published by Ghosh et al. [12]. The characteristics of the propagation of an elliptical step-index fiber with a conducting helical winding on the core-cladding boundary are investigated analytically [13]. The core and the cladding regions are assumed to have constant real refractive indices n_1 and n_2, where $n_1 > n_2$.

Calculation of the real and imaginary parts of the change in propagation constant of a surface-wave mode on a curved open waveguide of general cross section was proposed [14] in order to determine the quantities for TE mode of asymmetric slab waveguide, and for all the modes of an optical fiber.

Propagation in a curved rectangular waveguide with imperfect but smooth walls was proposed [15]. The lowest-order mode has a whispering gallery character, and the attenuation rate is increased significantly by the curvature. The computations of the modal characteristics are based on the Airy function approximation of the rigorous cylindrical wave functions.

The rectangular dielectric waveguide technique was proposed in order to determine the complex permittivity of a wide class of dielectric materials of various thicknesses and cross sections [16]. The technique enables to determine the dielectric constant of materials. The results indicate that the dielectric constant of samples of both small and large transverse dimensions can be determined with excellent accuracy by using the technique of the rectangular dielectric waveguide. A method to determine the complex permittivity and permeability of a material sample loaded in two rectangular waveguides was proposed [17]. The first waveguide terminated in a short and the second terminated in an open. A sample of the same cross section is placed in a short-circuit and an open-circuit position in two sections of the rectangular waveguide. The scattering parameters are measured for each case, and are used in order to determine the impedance at the face of the sample. These values of the impedance are used in an iterative method to solve for ϵ and μ.

The finite-element method based on whispering gallery modes in curved optical waveguides was proposed [18]. Numerical examples on the whispering gallery modes were given in a dielectric disk with rough boundaries. An approximate scalar finite-element method was applied for the analysis of whispering gallery modes. Rough boundaries of the disk have different effects on the angular propagation constant according to the position where the roughness exists. By increasing the width of the waveguide, the normal guided mode of the curved rectangular waveguide approaches to the whispering gallery modes in the disk waveguide. The minimum width of the curved rectangular waveguide increases with an increase of the curvature radius.

This paper presents the technique to solve inhomogeneous profiles in the cross section of the helical rectangular waveguide. The inhomogeneous examples will introduce for a dielectric slab, for a rectangular dielectric profile, and for a circular dielectric profile, in a rectangular metallic waveguide, in the cross section of the helical waveguide. The main steps of the derivation for the propagation along curved and helical waveguides are given in detail [19–21]. Thus we will introduce the main steps of the derivation in brief. The technique to solve inhomogeneous profiles will introduce in more detail. This proposed model is useful to improve the output results of the

output power transmission in the cases of space helical waveguides, by increasing the step's angle or the radius of the cylinder.

2. THE DERIVATION

Let us introduce the main steps of the derivation of the method of the propagation along a helical waveguide, in brief. The technique to solve inhomogeneous profiles in the cross section of the helical rectangular waveguide will be given after the derivation, in detail.

The helical and toroidal waveguides with a rectangular cross section are shown in Figs. 1(a) and 1(b), respectively. A general scheme of the curved coordinate system $(x,\ y,\ \zeta)$ is shown in Fig. 1(b), with the parameters R and $\delta_p \ll 1$, where R is the radius of the curvature of the toroidal waveguide and δ_p is the step's angle.

The metric coefficients in the case of the helical waveguide are:

$$h_x = 1, \tag{1a}$$

$$h_y = 1, \tag{1b}$$

$$\begin{aligned} h_\zeta &= \sqrt{\left(1+\frac{x}{R}\right)^2 \cos^2(\delta_p) + \sin^2(\delta_p)\left(1+\frac{y^2}{R^2}\cos^2(\delta_p)\right)} \\ &= \sqrt{1+\frac{2x}{R}\cos^2(\delta_p) + \frac{x^2}{R^2}\cos^2(\delta_p) + \frac{y^2}{R^2}\cos^2(\delta_p)\sin^2(\delta_p)} \\ &\simeq 1+\frac{x}{R}\cos^2(\delta_p), \end{aligned} \tag{1c}$$

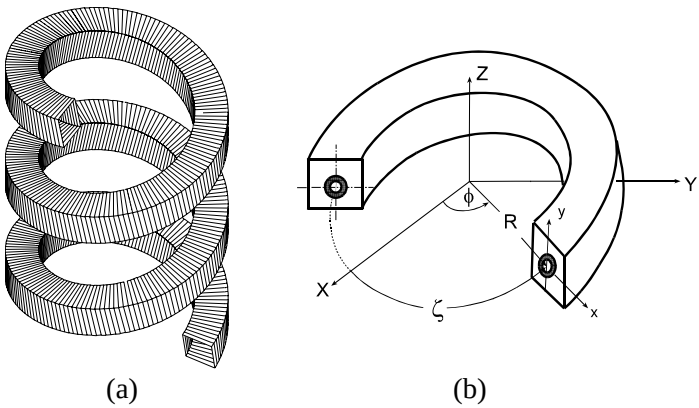

Figure 1. (a) The rectangular helical waveguide. (b) A general scheme of the curved coordinate system $(x,\ y,\ \zeta)$.

where R and δ_p are the radius of the cylinder and the step's angle of the helical waveguide, respectively. Note that the radius of the curvature of the toroidal waveguide (Fig. 1(b)) is generalized to the radius of the cylinder (R) of the helical waveguide (Fig. 1(a)). The first parameter of the helical waveguide relates to the radius of the cylinder (R), and the second parameter relates to the step's angle (δ_p), where the relevant values will be demonstrated in the output results for $0 \leq \delta_p \leq 1$.

The wave equations for the components of the electric and magnetic field are given by

$$\nabla^2\mathbf{E} + \omega^2\mu\epsilon\mathbf{E} + \nabla\left(\mathbf{E}\cdot\frac{\nabla\epsilon}{\epsilon}\right) = 0, \tag{2a}$$

and

$$\nabla^2\mathbf{H} + \omega^2\mu\epsilon\mathbf{H} + \frac{\nabla\epsilon}{\epsilon}\times(\nabla\times\mathbf{H}) = 0, \tag{2b}$$

where $\epsilon(x,y) = \epsilon_0(1+\chi_0 g(x,y))$, ϵ_0 is the vacuum dielectric constant, and χ_0 is the susceptibility.

The components of $\nabla^2\mathbf{E}$ are given by

$$(\nabla^2\mathbf{E})_x = \nabla^2 E_x - \frac{1}{R^2h_\zeta^2}\cos^2(\delta_p)E_x - 2\frac{1}{Rh_\zeta^2}\cos^2(\delta_p)\frac{\partial}{\partial\zeta}E_\zeta, \tag{3a}$$

$$(\nabla^2\mathbf{E})_y = \nabla^2 E_y, \tag{3b}$$

$$(\nabla^2\mathbf{E})_\zeta = \nabla^2 E_\zeta - \frac{1}{R^2h_\zeta^2}\cos^2(\delta_p)E_\zeta + 2\frac{1}{Rh_\zeta^2}\cos^2(\delta_p)\frac{\partial}{\partial\zeta}E_x, \tag{3c}$$

where

$$\nabla^2 = \frac{\partial^2}{\partial x^2} + \frac{\partial^2}{\partial y^2} + \frac{1}{h_\zeta^2}\frac{\partial^2}{\partial\zeta^2} + \frac{1}{Rh_\zeta}\cos^2(\delta_p)\frac{\partial}{\partial x}. \tag{4}$$

The wave Eqs. (2a) and (2b) are given by

$$\left(\nabla^2\mathbf{E}\right)_i + k^2E_i + \partial_i(E_xg_x + E_yg_y) = 0, \tag{5a}$$

$$\left(\nabla^2\mathbf{H}\right)_i + k^2H_i + \partial_i(H_xg_x + H_yg_y) = 0, \tag{5b}$$

where $i = x,\ y,\ \zeta$, $k = \omega\sqrt{\mu\epsilon(x,y)} = k_0\sqrt{1+\chi_0 g(x,y)}$, and $k_0 = \omega\sqrt{\mu_0\epsilon_0}$.

The transverse Laplacian operator is defined as $\nabla_\perp^2 = (1/h_\zeta^2)(\partial^2/\partial\zeta^2)$. The wave equations (Eqs. (2a)) are described in the Laplace transform as follows

$$h_\zeta^2\left(\nabla_\perp^2 + \frac{s^2}{h_\zeta^2} + k^2\right)\tilde{E}_x + h_\zeta^2\partial_x\left(\tilde{E}_xg_x + \tilde{E}_yg_y\right) + h_\zeta\frac{1}{R}\cos^2(\delta_p)\partial_x\left(\tilde{E}_x\right)$$
$$-\frac{2}{R}\cos^2(\delta_p)s\tilde{E}_\zeta = \left(sE_{x_0} + E'_{x_0}\right) - \frac{2}{R}\cos^2(\delta_p)E_{\zeta_0}, \tag{6}$$

and similarly, the other equations are given, where $E_{x_0} = E_x(x,\, y,\, \zeta = 0)$ and $E'_{x_0} = \frac{\partial}{\partial\zeta}E_x(x,y,\zeta)|_{\zeta=0}$. The differential equations are rewritten in a matrix form, where $\hat{E}_{x_0} = (s\bar{E}_{x_0} + \bar{E}'_{x_0})/2s$, $\hat{E}_{y_0} = (s\bar{E}_{y_0} + \bar{E}'_{y_0})/2s$, and $\hat{E}_{\zeta_0} = (s\bar{E}_{\zeta_0} + \bar{E}'_{\zeta_0})/2s$.

A Fourier transform is given by

$$\bar{g}(k_x,k_y) = \mathcal{F}\{g(x,y)\} = \int_x\int_y g(x,y)e^{-jk_xx-jk_yy}dxdy, \tag{7}$$

and the values $\mathbf{P^{(0)}}$ and $\mathbf{Q^{(0)}}$ are given as:

$$\bar{p_\zeta}^{(o)}_{(n,m)} = \frac{1}{4ab}\int_{-a}^{a}\int_{-b}^{b} p_\zeta(x)e^{-j\left(n\frac{\pi}{a}x+m\frac{\pi}{b}y\right)}dxdy, \tag{8a}$$

$$\bar{q_\zeta}^{(o)}_{(n,m)} = \frac{1}{4ab}\int_{-a}^{a}\int_{-b}^{b} q_\zeta(x)e^{-j\left(n\frac{\pi}{a}x+m\frac{\pi}{b}y\right)}dxdy, \tag{8b}$$

where

$$\mathbf{P^{(1)}} = \left(\mathbf{I} + \mathbf{P^{(0)}}\right), \tag{8c}$$

$$\mathbf{Q^{(1)}} = \left(\mathbf{I} + \mathbf{Q^{(0)}}\right), \tag{8d}$$

and where $\mathbf{I}$ is the unity matrix.

The modified wave-number matrices are given by

$$\mathbf{D_x} \equiv \mathbf{K^{(0)}} + \mathbf{Q^{(0)}K1^{(0)}} + \frac{k_o^2\chi_0}{2s}\mathbf{Q^{(1)}G} + \frac{jk_{ox}}{2s}\mathbf{Q^{(1)}NG_x} + \frac{1}{2sR}\cos^2(\delta_p)jk_{ox}\mathbf{P^{(1)}N}, \tag{9a}$$

$$\mathbf{D_y} \equiv \mathbf{K^{(0)}} + \mathbf{Q^{(0)}K1^{(0)}} + \frac{k_o^2\chi_0}{2s}\mathbf{Q^{(1)}G} + \frac{1}{2sR}\cos^2(\delta_p)jk_{ox}\mathbf{P^{(1)}N} + \frac{jk_{oy}}{2s}\mathbf{Q^{(1)}MG_y}, \tag{9b}$$

$$\mathbf{D}_\zeta \equiv \mathbf{K^{(0)}} + \mathbf{Q^{(0)}K1^{(0)}} + \frac{k_o^2\chi_0}{2s}\mathbf{Q^{(1)}G} + \frac{1}{2sR}\cos^2(\delta_p)jk_{ox}\mathbf{P^{(1)}N}, \tag{9c}$$

where the values of the diagonal matrices $\mathbf{K^{(0)}}$, $\mathbf{M}$, $\mathbf{N}$ and $\mathbf{K^{(1)}}$ are given by

$$K^{(0)}{}_{(n,m)(n',m')} = \left\{\left[k_o^2 - (n\pi/a)^2 - (m\pi/b)^2 + s^2\right]/2s\right\}\delta_{nn'}\delta_{mm'}, \tag{10a}$$

$$M_{(n,m)(n',m')} = m\delta_{nn'}\delta_{mm'}, \tag{10b}$$

$$N_{(n,m)(n',m')} = n\delta_{nn'}\delta_{mm'}, \tag{10c}$$

$$K^{(1)}{}_{(n,m)(n',m')} = \left\{\left[k_o^2 - (n\pi/a)^2 - (m\pi/b)^2\right]/2s\right\}\delta_{nn'}\delta_{mm'}. \tag{10d}$$

The components of the electric field are given by

$$E_x = \left\{ \mathbf{D_x} + \alpha_1 \mathbf{Q^{(1)}} \mathbf{M_1} \mathbf{Q^{(1)}} \mathbf{M_2} + \frac{1}{R}\cos^2(\delta_p) \mathbf{D_\zeta}^{-1} \left(-\frac{1}{2} \mathbf{Q^{(1)}} \mathbf{G_x} + \frac{1}{2}\alpha_2 \mathbf{Q^{(1)}} \mathbf{M_3} \mathbf{Q^{(1)}} \mathbf{M_2} - \frac{1}{R}\cos^2(\delta_p)\mathbf{I} \right) \right\}^{-1} \left(\hat{E}_{x_0} - \frac{1}{sR}\cos^2(\delta_p) E_{\zeta_0} - \alpha_3 \mathbf{Q^{(1)}} \mathbf{M_1} \hat{E}_{y_0} + \frac{1}{R}\cos^2(\delta_p) \mathbf{D_\zeta}^{-1} \left(\hat{E}_{\zeta_0} + \frac{1}{sR}\cos^2(\delta_p) E_{x_0} + \frac{1}{2s} \mathbf{Q^{(1)}} (\mathbf{G_x} E_{x_0} + \mathbf{G_y} E_{y_0}) - \frac{1}{2} \mathbf{Q^{(1)}} \mathbf{M_3} \hat{E}_{y_0} \right) \right), \tag{11a}$$

$$E_y = \mathbf{D_y}^{-1} \left(\hat{E}_{y_0} - \frac{jk_{oy}}{2s} \mathbf{Q^{(1)}} \mathbf{M} \mathbf{G_x} E_x \right), \tag{11b}$$

$$E_\zeta = \mathbf{D_\zeta}^{-1} \left\{ \hat{E}_{\zeta_0} + \frac{1}{2s} \mathbf{Q^{(1)}} (\mathbf{G_x} E_{x_0} + \mathbf{G_y} E_{y_0}) - \frac{1}{2} \mathbf{Q^{(1)}} (\mathbf{G_x} E_x + \mathbf{G_y} E_y) - \frac{1}{R}\cos^2(\delta_p) E_x + \frac{1}{sR}\cos^2(\delta_p) E_{x_0} \right\}, \tag{11c}$$

where:

$$\alpha_1 = \frac{k_{ox} k_{oy}}{4s^2}, \quad \alpha_2 = \frac{jk_{oy}}{2s}, \quad \alpha_3 = \frac{jk_{ox}}{2s}, \quad \mathbf{M_1} = \mathbf{N} \mathbf{G_y} \mathbf{D_y}^{-1},$$
$$\mathbf{M_2} = \mathbf{M} \mathbf{G_x}, \quad \mathbf{M_3} = \mathbf{G_y} \mathbf{D_y}^{-1}.$$

Similarly, the other components of the magnetic field are obtained. The output transverse field profiles are given by the inverse Laplace and Fourier transforms, as follows

$$E_y(x, y, \zeta) = \sum_n \sum_m \int_{\sigma - j_\infty}^{\sigma + j_\infty} E_y(n, m, s) e^{jnk_{ox}x + jmk_{oy}y + s\zeta} ds. \tag{12}$$

the inverse Laplace transforms is calculated according to the Salzer method [22, 23].

The ζ component of the average-power density is given by

$$S_{av} = \frac{1}{2} \mathrm{Re} \left\{ E_x {H_y}^* - E_y {H_x}^* \right\}. \tag{13}$$

A Fortran code is developed using NAG subroutines (The Numerical Algorithms Group (NAG)). Several inhomogeneous examples computed on a Unix system are presented in the next section.

3. NUMERICAL RESULTS

Several examples are demonstrated in this section. This paper presents the technique to solve inhomogeneous profiles in the cross section

of the helical rectangular waveguide. In this study, we find the inhomogeneous dielectric profiles in the cross section of importance examples and show the relation to the proposed method of the propagation of the electromagnetic fields along a helical waveguide with a rectangular cross section.

Two kinds of examples are demonstrated in this section, in order to understand the technique to solve inhomogeneous profiles in the helical metallic waveguide. The first example is given for a rectangular dielectric profile in the rectangular cross section of the helical waveguide. The second example is given for a circular dielectric profile in the rectangular cross section of the helical waveguide. Three kinds of interesting cases for inhomogeneous dielectric profiles in the cross section along the helical rectangular waveguide are shown in Figs. 2(a)–2(c). Fig. 2(a) shows a dielectric slab profile in a rectangular metallic waveguide. Fig. 2(b) shows a rectangular dielectric profile loaded in the rectangular metallic waveguide. Fig. 2(c) shows a circular dielectric profile in the rectangular waveguide.

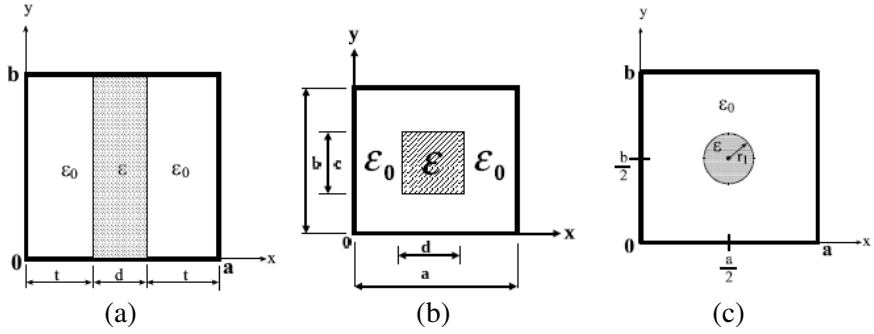

Figure 2. (a) A dielectric slab profile in a rectangular metallic waveguide. (b) A rectangular dielectric profile in a rectangular metallic waveguide. (c) A circular dielectric profile in a rectangular metallic waveguide.

3.1. Example 1: A Rectangular Dielectric Profile

Three interesting examples are demonstrated in Figs. 2(a)–2(c), in order understand the proposed technique to solve inhomogeneous dielectric profiles in the cross section of the rectangular cross section of the helical waveguide.

The ω_ε function [24] is used in order to solve discontinuous problems in the cross section of the helical waveguide. The ω_ε function

(Fig. 3(a)) is defined as

$$\omega_\varepsilon(r) = \begin{cases} C_\varepsilon e^{-\frac{\varepsilon^2}{\varepsilon^2-|r|^2}} & |r| \le \varepsilon \\ 0 & |r| > \varepsilon \end{cases}, \tag{14}$$

where C_ε is a constant, and $\int \omega_\varepsilon(r)dr = 1$.

In the limit $\varepsilon \longrightarrow 0$, the ω_ε function (Eq. (14)) is shown in Fig. 3(b). Fig. 4 shows an example of the inhomogeneous profile in the rectangular cross section of the helical waveguide for $g(x)$ function. In order to solve inhomogeneous dielectric profiles we use with ω_ε function, with the parameters ε_1 and ε_2.

In order to solve inhomogeneous dielectric profiles (e.g., in Figs. 2(a)–2(c)) in the cross section of the helical waveguide, the parameters ε_1 and ε_2 are used according to the ω_ε function (Figs. 3(a) and 3(b)), where $\varepsilon_1 \longrightarrow 0$ and $\varepsilon_2 \longrightarrow 0$. The dielectric profiles for a rectangular dielectric profile in the rectangular cross section (Fig. 2(b)) are given by

$$g(x) = \begin{cases} 0 & 0 \le x < (a-d-\varepsilon_1)/2 \\ g_0 \exp\left[1 - \frac{{\varepsilon_1}^2}{\varepsilon_1^2 - [x-(a-d+\varepsilon_1)/2]^2}\right] & (a-d-\varepsilon_1)/2 \le x < (a-d+\varepsilon_1)/2 \\ g_0 & (a-d+\varepsilon_1)/2 < x < (a+d-\varepsilon_2)/2 \\ g_0 \exp\left[1 - \frac{{\varepsilon_2}^2}{{\varepsilon_2}^2 - [x-(a+d-\varepsilon_2)/2]^2}\right] & (a+d-\varepsilon_2)/2 \le x < (a+d+\varepsilon_2)/2 \\ 0 & (a+d+\varepsilon_2)/2 < x \le a \end{cases}, \tag{15a}$$

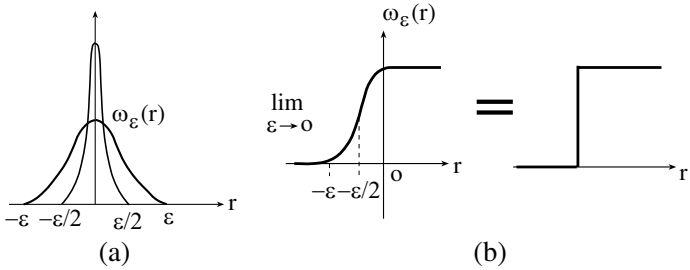

Figure 3. (a) The ω_ε function. (b) The ω_ε function in the limit $\varepsilon \to 0$.

and

$$g(y)=\begin{cases} 0 & 0 \le y < (b-c-\varepsilon_1)/2 \\ g_0 \exp\left[1-\dfrac{{\varepsilon_1}^2}{{\varepsilon_1}^2-[y-(b-c+\varepsilon_1)/2]^2}\right] & (b-c-\varepsilon_1)/2 \le y < (b-c+\varepsilon_1)/2 \\ g_0 & (b-c+\varepsilon_1)/2 < y < (b+c-\varepsilon_2)/2\,. \\ g_0 \exp\left[1-\dfrac{{\varepsilon_2}^2}{{\varepsilon_2}^2-[y-(b+c-\varepsilon_2)/2]^2}\right] & (b+c-\varepsilon_2)/2 \le y < (b+c+\varepsilon_2)/2 \\ 0 & (b+c+\varepsilon_2)/2 < y \le b \end{cases} \tag{15b}$$

The elements of the matrix $g(n, m)$ are given according to Fig. 2(b), in the case of $b \neq c$ by

$$\begin{aligned} g(n,m)=\frac{g_0}{ab}\Bigg\{ & \int_{(a-d-\varepsilon_1)/2}^{(a-d+\varepsilon_1)/2} \exp\left[1-\frac{{\varepsilon_1}^2}{{\varepsilon_1}^2-[x-(a-d+\varepsilon_1)/2]^2}\right]\cos\left(\frac{n\pi x}{a}\right)dx \\ & + \int_{(a-d+\varepsilon_1)/2}^{(a+d-\varepsilon_2)/2} \cos\left(\frac{n\pi x}{a}\right)dx + \int_{(a+d-\varepsilon_2)/2}^{(a+d+\varepsilon_2)/2} \\ & \exp\left[1-\frac{{\varepsilon_2}^2}{{\varepsilon_2}^2-[x-(a+d-\varepsilon_2)/2]^2}\right]\cos\left(\frac{n\pi x}{a}\right)dx\Bigg\} \\ & \Bigg\{\int_{(b-c-\varepsilon_1)/2}^{(b-c+\varepsilon_1)/2} \exp\left[1-\frac{{\varepsilon_1}^2}{{\varepsilon_1}^2-[y-(b-c+\varepsilon_1)/2)]^2}\right]\cos\left(\frac{m\pi y}{b}\right)dy \\ & + \int_{(b-c+\varepsilon_1)/2}^{(b+c-\varepsilon_2)/2} \cos\left(\frac{m\pi y}{b}\right)dy + \int_{(b+c-\varepsilon_2)/2}^{(b+c+\varepsilon_2)/2} \\ & \exp\left[1-\frac{{\varepsilon_2}^2}{{\varepsilon_2}^2-[y-(b+c-\varepsilon_2)/2)]^2}\right]\cos\left(\frac{m\pi y}{b}\right)dy\Bigg\}. \end{aligned} \tag{16}$$

The elements of the matrix $g(n, m)$ (Eq. (16)) are given according to Fig. 2(a), in the case of $b = c$ by

$$g(n,m)=\frac{g_0}{ab}\left\{\int_{(a-d-\varepsilon_1)/2}^{(a-d+\varepsilon_1)/2} \exp\left[1-\frac{{\varepsilon_1}^2}{{\varepsilon_1}^2-[x-(a-d+\varepsilon_1)/2]^2}\right]\cos\left(\frac{n\pi x}{a}\right)dx\right.$$

$$+\int_{(a-d+\varepsilon_1)/2}^{(a+d-\varepsilon_2)/2}\cos\left(\frac{n\pi x}{a}\right)dx+\int_{(a+d-\varepsilon_2)/2}^{(a+d+\varepsilon_2)/2}$$
$$\exp\left[1-\frac{{\varepsilon_2}^2}{{\varepsilon_2}^2-[x-(a+d-\varepsilon_2)/2]^2}\right]\cos\left(\frac{n\pi x}{a}\right)dx\Bigg\}\left\{\int_0^b\cos\left(\frac{m\pi y}{b}\right)dy\right\}.$$

The derivatives of the dielectric profile are given by

$$g_x \equiv \frac{1}{\epsilon(x,y)}\frac{\partial\epsilon(x,y)}{\partial x} = \frac{\partial[\ln(1+g(x,y))]}{\partial x}, \tag{17a}$$

$$g_y \equiv \frac{1}{\epsilon(x,y)}\frac{\partial\epsilon(x,y)}{\partial y} = \frac{\partial[\ln(1+g(x,y))]}{\partial y}. \tag{17b}$$

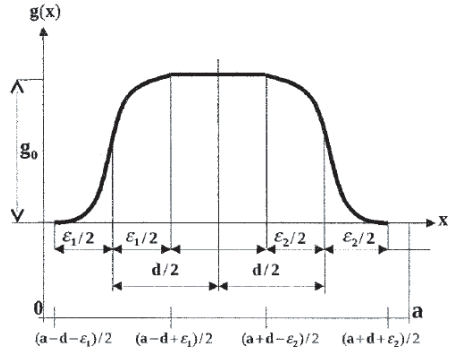

Figure 4. An example of the inhomogeneous profile in the rectangular cross section for $g(x)$ function with the parameters ε_1 and ε_2.

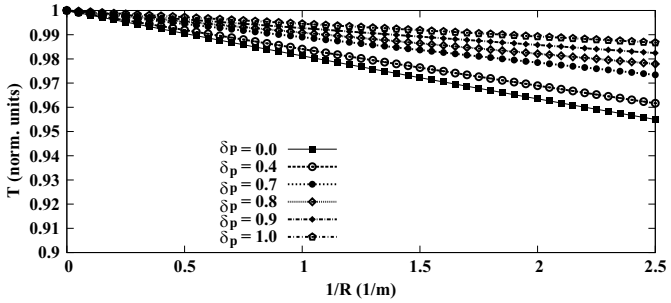

Figure 5. The output power transmission as a function of $1/R$ and δ_p ($\delta_p = 0.0$, 0.4, 0.7, 0.8, 0.9, 1.0).

Thus,

$$g_x=\begin{cases}0 & 0\le x<(a-d-\varepsilon_1)/2\\ \dfrac{d}{dx}\left\{\ln\left[1+g_0\exp\left[1-\dfrac{{\varepsilon_1}^2}{{\varepsilon_1}^2-[x-(a-d+\varepsilon_1)/2]^2}\right]\right]\right\} & (a-d-\varepsilon_1)/2\le x<(a-d+\varepsilon_1)/2\\ 0 & (a-d+\varepsilon_1)/2<x<(a+d-\varepsilon_2)/2\\ \dfrac{d}{dx}\left\{\ln\left[1+g_0\exp\left[1-\dfrac{{\varepsilon_2}^2}{{\varepsilon_2}^2-[x-(a+d-\varepsilon_2)/2]^2}\right]\right]\right\} & (a+d-\varepsilon_2)/2\le x<(a+d+\varepsilon_2)/2\\ 0 & (a+d+\varepsilon_2)/2<x\le a\end{cases}, \quad (18a)$$

$$g_y=\begin{cases}0 & 0\le y<(b-c-\varepsilon_1)/2\\ \dfrac{d}{dx}\left\{\ln\left[1+g_0\exp\left[1-\dfrac{{\varepsilon_1}^2}{{\varepsilon_1}^2-[y-(b-c+\varepsilon_1)/2]^2}\right]\right]\right\} & (b-c-\varepsilon_1)/2\le y<(b-c+\varepsilon_1)/2\\ 0 & (b-c+\varepsilon_1)/2<y<(b+c-\varepsilon_2)/2\\ \dfrac{d}{dx}\left\{\ln\left[1+g_0\exp\left[1-\dfrac{{\varepsilon_2}^2}{{\varepsilon_2}^2-[y-(b+c-\varepsilon_2)/2]^2}\right]\right]\right\} & (b+c-\varepsilon_2)/2\le x<(b+c+\varepsilon_2)/2\\ 0 & (b+c+\varepsilon_2)/2<y\le b\end{cases}. \quad (18b)$$

The results of output power transmission as function of $1/R$ and $\delta_p = (0.0, 0.4, 0.7, 0.8, 0.9, 1.0)$ are demonstrated in Fig. 5, where $\zeta = 15\,\text{cm}$, $a = 2\,\text{cm}$, $b = c = 2\,\text{cm}$, $d = 1.6\,\text{cm}$, $\lambda = 3.75\,\text{cm}$, and $\epsilon_r = 1.5$, in the practical case of the slab dielectric profile (Fig. 2(a)). By increasing the parameters of the helical waveguide (δ_p and R), the results of the output power transmission are improved. Thus, this model is useful to improve the output results in the cases of space curved waveguides.

The result of the output power density (S_{av}) as function of ϵ_r is shown in Fig. 6(a) in the case of the slab dielectric profile ($a = 20\,\text{mm}$, $b = c = 20\,\text{mm}$, and $d = 16\,\text{mm}$), where $\epsilon_r = 1.5$. The result

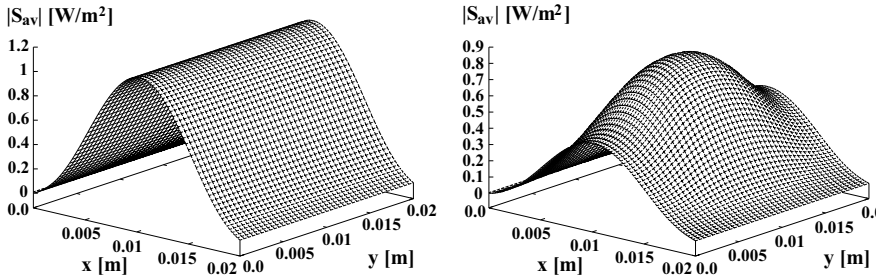

Figure 6. (a) The output power density as function of ϵ_r in the case of the slab dielectric profile ($a = 20\,\text{mm}$, $b = c = 20\,\text{mm}$, and $d = 16\,\text{mm}$), where $\epsilon_r = 1.5$. (b) The result of the rectangular dielectric profile in the rectangular cross section ($a = b = 20\,\text{mm}$, and $c = d = 16\,\text{mm}$), where $\epsilon_r = 2.0$. The other parameters are $\lambda = 3.75$ cm, $\delta_p = 1$, $R = 0.26$ m, and $\zeta = 15$ cm.

of the output power density as function of ϵ_r is shown in Fig. 6(b) for the rectangular dielectric profile in the rectangular cross section, where $a = b = 20\,\text{mm}$, $c = d = 16\,\text{mm}$, and $\epsilon_r = 2.0$. The other parameters are given for $\delta_p = 1$, and $R = 0.26\,\text{m}$, where $\zeta = 15\,\text{cm}$, and $\lambda = 3.75\,\text{cm}$. The result in Fig. 6(b) is shown for TE_{10} mode and the rectangular dielectric profile in the rectangular metallic waveguide (Fig. 2(b)).

The amplitude of the output power density and the output profile shape for four values of $\epsilon_r = 1.5$, 1.6, 1.75, and 2.0, respectively, are shown in Fig. 7(a). The output profile is shown in the same cross section of output transverse profile of Fig. 6(a), where $y = b/2 = 10\,\text{mm}$. An example for the output profiles for $N = 1$, 3, 5 and 7, is shown in Fig. 7(b), where $\epsilon_r = 1.5$. The output power density approaches to the final output power density, by increasing only the parameter of the order N.

3.2. Example 2: A Circular Dielectric Profile

An example of the cross section of a circular dielectric profile in the metallic waveguide is demonstrated in Fig. 2(c) for an inhomogeneous dielectric profile, where r_1 is the radius of the circle, and a and b are the dimensions of the cross-section. The refractive index of the cladding (air) is smaller than that of the core (dielectric profile). The center of the circle (Fig. 2(c)) located at the point ($a/2$, $b/2$). The dielectric

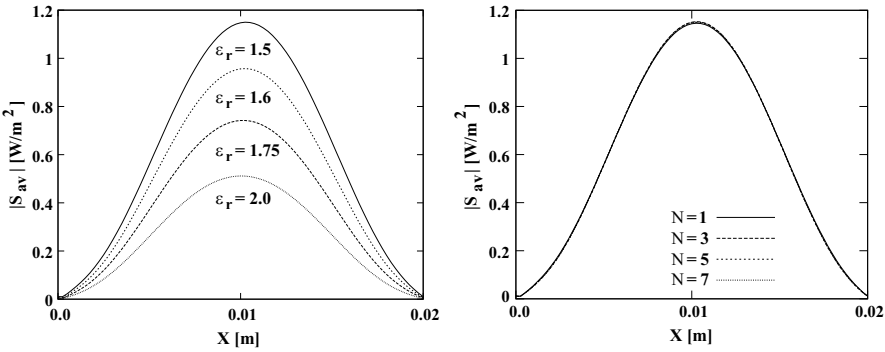

Figure 7. (a) The output power density in the same cross section of Fig. 6(a) where $y = b/2 = 10\,\text{mm}$, in the case of the slab dielectric profile ($a = 20\,\text{mm}$, $b = c = 20\,\text{mm}$, and $d = 16\,\text{mm}$), for $\delta_p = 1$, $R = 0.26\,\text{m}$, and for some values of ϵ_r. (b) The output profile for $N = 1$, 3, 5, and 7, where $\epsilon_r = 1.5$.

profile is given by

$$g(x,y) = \begin{cases} g_0 & 0 \le r < r_1 - \varepsilon_1/2 \\ g_0 \exp\left[1 - \dfrac{{\varepsilon_1}^2}{{\varepsilon_1}^2 - [r - (r_1 - \varepsilon_1/2)]^2}\right] & r_1 - \varepsilon_1/2 \le r < r_1 + \varepsilon_1/2 \\ 0 & \text{else} \end{cases}, \quad (19)$$

where $r = \sqrt{(x - a/2)^2 + (y - b/2)^2}$.

Thus, the derivatives are given by

$$g_x = \begin{cases} 0 & 0 \le r < r_1 - \varepsilon_1/2 \\ -2g_0 \cos\theta \exp\left[1 - \dfrac{{\varepsilon_1}^2}{{\varepsilon_1}^2 - [r - (r_1 - \varepsilon_1/2)]^2}\right] & \\ \dfrac{[r - (r_1 - \varepsilon_1/2)]{\varepsilon_1}^2}{\left\{1 + g_0 \exp\left[1 - \dfrac{{\varepsilon_1}^2}{{\varepsilon_1}^2 - [r - (r_1 - \varepsilon_1/2)]^2}\right]\right\} \left[{\varepsilon_1}^2 - [r - (r_1 - \varepsilon_1/2)]^2\right]^2} & r_1 - \varepsilon_1/2 \le r < r_1 + \varepsilon_1/2 \\ 0 & \text{else} \end{cases}, \quad (20a)$$

$$g_y = \begin{cases} 0 & 0 \le r < r_1 - \varepsilon_1/2 \\ -2\ g_0 \sin\theta \exp\left[1 - \dfrac{{\varepsilon_1}^2}{{\varepsilon_1}^2 - [r-(r_1-\varepsilon_1/2)]^2}\right] & \\ \dfrac{[r-(r_1-\varepsilon_1/2)]{\varepsilon_1}^2}{\left\{1+g_0 \exp\left[1-\dfrac{{\varepsilon_1}^2}{{\varepsilon_1}^2-[r-(r_1-\varepsilon_1/2)]^2}\right]\right\}} & r_1-\varepsilon_1/2 \le r \\ \left[{\varepsilon_1}^2-[r-(r_1-\varepsilon_1/2)]^2\right]^2 & < r_1+\varepsilon_1/2 \\ 0 & \text{else} \end{cases} . \quad (20b)$$

The elements of the matrices in the limit $\varepsilon_1 = \varepsilon \to 0$ are given by

$$g(n,m) = \frac{g_0}{ab}\left\{\int_0^{2\pi}\int_0^{r_1-\epsilon/2} \cos\left[\frac{n\pi}{a}\left(r\cos\theta+\frac{a}{2}\right)\right]\cos\left[\frac{m\pi}{b}\left(r\sin\theta+\frac{b}{2}\right)\right] + \int_0^{2\pi}\int_{r_1-\epsilon/2}^{r_1+\epsilon/2} \cos\left[\frac{n\pi}{a}\left(r\cos\theta+\frac{a}{2}\right)\right]\cos\left[\frac{m\pi}{b}\left(r\sin\theta+\frac{b}{2}\right)\right] \exp\left[1-\frac{\epsilon^2}{\epsilon^2-[r-(r_1-\epsilon/2)]^2}\right]\right\} r\,dr\,d\theta, \quad (21)$$

$$g_x(n,m) = -\frac{2g_0}{ab}\left\{\int_0^{2\pi}\int_{r_1-\epsilon/2}^{r_1+\epsilon/2} \frac{\exp\left[1-\dfrac{\epsilon^2}{\epsilon^2-[r-(r_1-\epsilon/2)]^2}\right]\cos\theta}{\left[\epsilon^2-[r-(r_1-\epsilon/2)]^2\right]^2} \left[1+g_0\exp\left[1-\frac{\epsilon^2}{\epsilon^2-[r-(r_1-\epsilon/2)]^2}\right]\right] \cos\left[\frac{n\pi}{a}\left(r\cos\theta+\frac{a}{2}\right)\right]\cos\left[\frac{m\pi}{b}(r\sin\theta+\frac{b}{2})\right]\right\} r\,dr\,d\theta, \quad (22a)$$

$$g_y(n,m) = -\frac{2g_0}{ab}\left\{\int_0^{2\pi}\int_{r_1-\epsilon/2}^{r_1+\epsilon/2} \frac{\exp\left[1-\dfrac{\epsilon^2}{\epsilon^2-[r-(r_1-\epsilon/2)]^2}\right]\sin\theta}{\left[\epsilon^2-[r-(r_1-\epsilon/2)]^2\right]^2} \left[1+g_0\exp\left[1-\frac{\epsilon^2}{\epsilon^2-[r-(r_1-\epsilon/2)]^2}\right]\right] \cos\left[\frac{n\pi}{a}\left(r\cos\theta+\frac{a}{2}\right)\right]\cos\left[\frac{m\pi}{b}\left(r\sin\theta+\frac{b}{2}\right)\right]\right\} r\,dr\,d\theta, \quad (22b)$$

where $r = \sqrt{(x-a/2)^2+(y-b/2)^2}$.

The results of the output power transmission as functions of $1/R$ and $\delta_p = (0.0, 0.4, 0.7, 0.8, 0.9, 1.0)$ are demonstrated in Fig. 8, where $\zeta = 15\,\text{cm}$, $a = b = 2\,\text{cm}$, $r_1 = 0.5\,\text{mm}$, $\lambda = 3.75\,\text{cm}$, and $\epsilon_r = 10$. These output results are dependent on the TE_{10} mode (the input wave profile) and the circular dielectric profile in the metallic waveguide (Fig. 2(c)). By increasing the parameters of the helical waveguide (δ_p and R), the results of the output power transmission are improved. Thus, this model is useful to improve the output results in the cases of space curved waveguides.

The results of the output power density for $\delta_p = 1$ and $R = 0.5\,\text{m}$ are shown in Figs. 9(a)–(b), where $\zeta = 15\,\text{cm}$, $a = b = 2\,\text{cm}$, $r_1 = 0.5\,\text{mm}$, and $\lambda = 3.75\,\text{cm}$. The amplitude of the output power density and the Gaussian shape in the same cross section of Figs. 9(a)–(b) are shown in Fig. 10(a), where $y = b/2 = 1\,\text{cm}$, and for $\epsilon_r = 2$, 5, 6, 8, and 10. By increasing only the parameter ϵ_r (Fig. 10(a)),

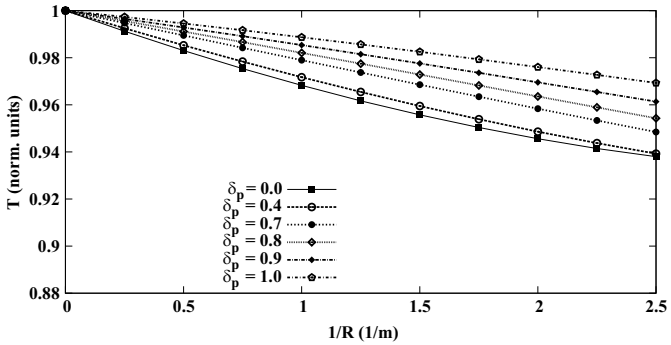

Figure 8. The output power transmission as a function of $1/R$ and $\delta_p = (0.0, 0.4, 0.7, 0.8, 0.9, 1.0)$.

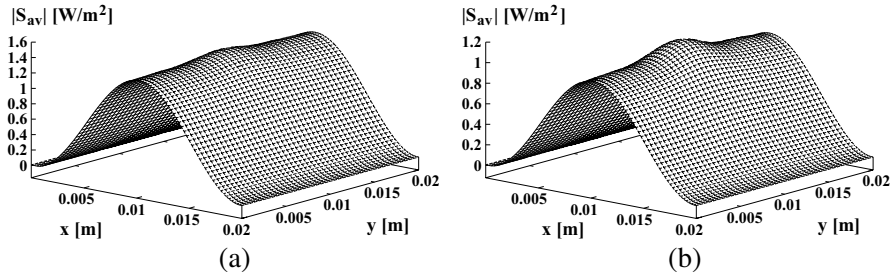

Figure 9. The output power density for $\delta_p = 1$, and $R = 0.5\,\text{m}$. (a) $\varepsilon_r = 5$. (b) $\varepsilon_r = 10$.

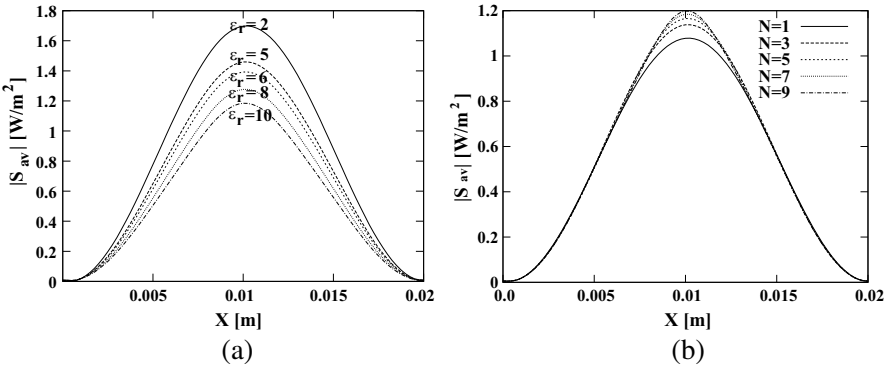

Figure 10. (a) The output power density in the same cross section of Figs. 9(a)–(b) for $\delta_p = 1$ and $R = 0.5$ m, and for some values of ϵ_r. (b) The output profile for $N = 1$, 3, 5, 7 and 9, where $\epsilon_r = 10$.

the output power density shows a Gaussian shape and the amplitude decreases. The dielectric profile for an inhomogeneous cross section is demonstrated in these examples for arbitrary values of δ_p and R of the helical waveguide.

An example for the output profiles with $\epsilon_r = 10$ is shown in Fig. 10(b) for the same other parameters of Figs. 9(a)–(b) and 10(a) and for every order ($N = 1$, 3, 5, 7, and 9). The output power density approaches to the final output power density, by increasing only the parameter of the order N.

4. CONCLUSIONS

The objective of this paper was to present the technique to solve inhomogeneous profiles (Figs. (2a)–2(c)) in the cross section of the helical rectangular waveguide. The inhomogeneous examples were introduced for a dielectric slab, for a rectangular dielectric profile, and for a circular dielectric profile, in a rectangular metallic waveguide, in the cross section of the helical waveguide. In order to solve inhomogeneous problems, the ω_ε function (Eq. (14)) is used.

The output power transmission as function of $1/R$ and δ_p is demonstrated in Figs. 5 and 8. By increasing the parameters of the helical waveguide (δ_p and R), the results of the output power transmission are improved. Thus, this model is useful to improve the output results in the cases of space curved waveguides.

Two examples are demonstrated to understand the technique to solve inhomogeneous profiles in the cross section along the helical waveguide. Fig. 2(a) shows a dielectric slab profile in a rectangular

metallic waveguide. Fig. 2(b) shows a rectangular dielectric profile loaded in the rectangular metallic waveguide. Fig. 2(c) shows a circular dielectric profile in the rectangular metallic waveguide.

Figure 6(a) shows the result of the output power density as function of ϵ_r in the case of the slab dielectric profile (Fig. 2(a)). Fig. 6(b) shows the result of the output power density as function of ϵ_r in the case of the rectangular dielectric profile in the rectangular metallic waveguide.

The output amplitude and the output profile shape of the output power density are shown in Fig. 7(a) for four values of $\epsilon_r = 1.5$, 1.6, 1.75, and 2.0, respectively. An example for the output profiles for $N = 1$, 3, 5 and 7 is shown in Fig. 7(b), where $\epsilon_r = 1.5$.

The results of the output power density for $\delta_p = 1$ and $R = 0.5\,\mathrm{m}$ are shown in Figs. 9(a)–(b). The results of the output fields are shown for TE_{10} mode and for the rectangular dielectric profile in the rectangular metallic waveguide (Fig. 2(c)). The amplitude of the output power density and the Gaussian shape of the central peak in the same cross section of Figs. 9(a)–(b) are shown in Fig. 10(a) for some values of ϵ_r. The output power density shows a Gaussian shape, by increasing only the parameter ϵ_r. The dielectric profile for an inhomogeneous cross section is demonstrated in these examples for arbitrary values of δ_p and R. The examples of the output power density for $\delta_p = 1$ and $R = 0.5\,\mathrm{m}$ are shown for some values of ϵ_r (Fig. 10(a)) and for some values of N (Fig. 10(b)).

This model is useful for helical rectangular waveguide with inhomogeneous dielectric profiles in the cross section. This model is used to find the parameters (δ_p and R) in order to improve the results of the output power transmission of the curved and helical waveguides.

REFERENCES

1. Riess, K., "Electromagnetic waves in a bent pipe of rectangular cross section," *Q. Appl. Math.*, Vol. 1, 328–333, 1944.
2. Trang, N. T. and R. Mittra, "Field profile in a single-mode curved dielectric waveguide of rectangular cross section," *IEEE Trans. on Microwave Theory and Tech.*, Vol. 29, 1315–1318, 1981.
3. Cochran, J. A. and R. G. Pecina, "Mode propagation in continuously curved waveguides," *Radio Science*, Vol. 1 (new series), No. 6, 679–696, 1966.
4. Carle, P. L., "New accurate and simple equivalent circuit for circular E-plane bends in rectangular waveguide," *Electronics Letters*, Vol. 23, No. 10, 531–532, 1987.

5. Weisshaar, A., S. M. Goodnick, and V. K. Tripathi, "A rigorous and efficient method of moments solution for curved waveguide bends," *IEEE Trans. on Microwave Theory and Tech.*, Vol. 40, No. 12, 2200–2206, 1992.
6. Cornet, P., R. Duss'eaux, and J. Chandezon, "Wave propagation in curved waveguides of rectangular cross section," *IEEE Trans. on Microwave Theory and Tech.*, Vol. 47, No. 7, 965–972, 1999.
7. Heiblum, M. and J. H. Harris, "Analysis of curved optical waveguides by conformal transformation," *IEEE J. Quantum Electron.*, Vol. 11, 75–83, 1975, Correction, ibid., Vol. 12, 313, 1975.
8. Kawakami, S., M. Miyagi, and S. Nishida, "Bending losses of dielectric slab optical waveguide with double or multiple claddings," *Appl. Optics*, Vol. 14, 2588–2597, 1975. Correction, ibid., Vol. 15, 1681, 1976.
9. Chang, D. C. and E. F. Kuester, "Radiation and propagation of a surface-wave mode on a curved open waveguide of arbitrary cross section," *Radio Science*, 449–457, 1976.
10. Marcatily, E. A. J. and R. A. Schmeltzer, "Hollow metallic and dielectric waveguides for long distance optical transmission and lasers," *Bell Syst. Tech. J.*, Vol. 43, 1783–1809, 1964.
11. Lewin, L., D. C. Chang, and E. F. Kuester, *Electromagnetic Waves and Curved Structures*, Chap. 8, 95–113, Peter Peregrinus Ltd., 1977.
12. Ghosh, S., P. K. Jain, and B. N. Basu, "Fast-wave analysis of an inhomogeneously-loaded helix enclosed in a cylindrical waveguide," *Progress In Electromagnetics Research*, Vol. 18, 19–43, 1998.
13. Kumar, D. and O. N. Singh II, "Elliptical and circular step-index with conducting helical windings on the core-cladding boundaries for the different winding pitch angles — A comparative modal dispersion analysis," *Progress In Electromagnetics Research*, Vol. 52, 1–21, 2005.
14. Kuester, E. F. and D. C. Chang, "Surface wave radiation loss from curved dielectric slabs and fibers," *J. Quantum Electron.*, Vol. 11, 903–907, 1975.
15. Mahmoud, S. F. and J. R. Wait, "Guided electromagnetic waves in a curved rectangular mine tunnel," *Radio Science*, Vol. 9, 567–572, 1974.
16. Abbas, Z., R. D. Pollard, and R. W. Kelsall, "A rectangular dielectric waveguide technique for determination of permittivity

of materials at W-band," *IEEE Trans. on Microwave Theory and Tech.*, Vol. 46, No. 12, 2011–2015, 1998.

17. Wolfson, B. J. and S. M. Wentworth, "Complex permittivity and permeability measurement using a rectangular waveguide," *Microwave and Optical Technology Letters*, Vol. 27, No. 3, 433–452, 2000.
18. Yamamoto, T. and M. Koshiba, "Analysis of propagation characteristics of whispering gallery modes in a dielectric disk or a curved rectangular dielectric waveguide," *Journal of Lightwave Technology*, Vol. 11, 400–404, 1993.
19. Menachem, Z., "Wave propagation in a curved waveguide with arbitrary dielectric transverse profiles — Abstract," *Journal of Electromagnetic Waves and Aplications*, Vol. 17, No. 10, 1423–1424, 2003.
20. Menachem, Z., "Wave propagation in a curved waveguide with arbitrary dielectric transverse profiles," *Progress In Electromagnetics Research*, Vol. 42, 173–192, 2003.
21. Menachem Z. and S. Tapuchi, "Wave propagation in a helical waveguide with slab and rectangular dielectric profiles and applications," *Progress In Electromagnetics Research B*, Vol. 34, 77–102, 2011.
22. Salzer, H. E., "Orthogonal polynomials arising in the numerical evaluation of inverse Laplace transforms," *Math. Tables and Other Aids to Comut.*, Vol. 9, 164–177, 1955.
23. Salzer, H. E., "Additional formulas and tables for orthogonal polynomials originating from inversion integrals," *J. Math. Phys.*, Vol. 39, 72–86, 1961.
24. Vladimirov, V., *Equations of Mathematical Physics*, 1971.